Clays and Clay Minerals, Vol. 57, No. 5, 566–577, 2009.

PROGRESSIVE FORMATION OF HALLOYSITE FROM THE HYDROTHERMAL ALTERATION OF BIOTITE AND THE FORMATION MECHANISMS OF ANATASE IN ALTERED VOLCANIC ROCKS FROM LIMNOS ISLAND, NORTHEAST AEGEAN SEA, GREECE

DIMITRIOS PAPOULIS[1], PANAGIOTA TSOLIS-KATAGAS[1], ANGELOS G. KALAMPOUNIAS[2,3], AND BASILIOS TSIKOURAS[1]

[1] Department of Geology, Section of Earth Materials, University of Patras, GR-26504 Patras, Greece
[2] Department of Chemical Engineering, University of Patras, P.O. Box 1414, GR -26504 Patras, Greece
[3] Institute of Chemical Engineering and High Temperature Chemical Processes (FORTH/ICE-HT), GR-26504 Patras, Greece

Abstract—Occurrences of halloysite-rich material in altered volcanic rocks, principally trachyandesites, dacites, and tuffs, extend over an area of ~1 km^2 in the southwestern part of Limnos, Island, northeast Aegean Sea, Greece. The present study was designed to investigate the alteration processes which acted on the biotite in these volcanic rocks, to describe in detail the mechanism of formation of the halloysite, and to specify the mechanisms of formation of anatase during the alteration processes. Samples were examined using polarized-light microscopy, X-ray powder diffraction, scanning electron microscopy, scanning electron microscopy-energy dispersive spectroscopy, and Fourier-transform-Raman techniques. The extensive alteration of the parent rocks, triggered by the circulation of hydrothermal fluids through faults and fractures, resulted in the alteration of biotite to halloysite. Six stages of alteration were recognized. Nanoparticles of halloysite were initially formed on the mica layers, which progressively grew through short-tubular to well formed tubular halloysite, with increasing alteration. In the most altered samples, laths and interconnected laths with the composition $(Al_{3.96}Fe_{0.04})Si_4O_{10}(OH)_8$, were the dominant halloysite morphologies. Anatase was encountered as an alteration product of both ilmenite and biotite. Ilmenite was altered to anatase and Fe oxides. The altered ilmenite crystals constrained most of the newly formed anatase within the space occupied previously by ilmenite, leading to the formation of skeletal anatase. The layered structure of the micas was the main factor governing the morphology of newly formed anatase developed outside ilmenite margins in the form of layers parallel to those of mica. An unusual ring-like structure of anatase was thought to be the result of the uncommon alteration of inner parts of mica folia to tubular halloysite oriented perpendicular to the mica layers. The detachment of the halloysite tubes by circulating hydrothermal fluids was considered to be the reason for the creation of holes which were subsequently surrounded by the anatase ring forms.

Key Words—Anatase, Biotite, Greece, Halloysite, Hydrothermal alteration, Limnos, SEM.

INTRODUCTION

Micas can alter to a variety of products, including vermiculite, smectite, chlorite, gibbsite, kaolinite, corrensite, and halloysite, depending upon the environment (*e.g.* Banfield and Eggleton, 1990; Jiang and Peacor, 1991; Dong *et al.*, 1998; Arostegui *et al.*, 2001; Ece and Schroeder, 2007). Previous investigations revealed that micas can alter by weathering to both halloysite and kaolinite (*e.g.* Jolicoeur *et al.*, 2000; Papoulis *et al.*, 2004a), while Ahn and Peacor (1987) ascribed the transition of one biotite layer to two kaolinite layers to hydrothermal fluids. Tubular halloysite is commonly derived from crystalline minerals, such as biotite (Singh and Gilkes, 1992), generally involving crystallization from solutions rather than topotactic alteration (Kirkman, 1981; Giese, 1988; Dixon, 1989; Chen *et al.*, 1997). Recent studies revealed the alteration of biotite, parallel to basal surfaces, to elongated halloysite in both weathering (*e.g.* Papoulis *et al.*, 2004a) and hydrothermal environments (Ece and Schroeder, 2007; Ece *et al.*, 2008). While the progressive alteration of biotite to halloysite and kaolinite has been studied by many scientists (*e.g.* Dong *et al.*, 1998), few studies, to our knowledge, have focused on the formation of halloysite from the hydrothermal alteration of biotite.

The small amounts of Ti that are commonly found in halloysite- and kaolinite-rich soils have been assigned to discrete oxides such as anatase or maghemite (Weaver, 1976; Quantin *et al.*, 1988; Schroeder and Shiflet, 2000; Joussein *et al.*, 2005), while TiO_2 found in hydrothermal halloysite and kaolinite occurrences may be concentrated in anatase by hydrothermal fluids (Murray and Keller, 1993; Harvey and Murray, 1993). Dill *et al.* (1997) suggested that Ti is released from its primary host minerals (*e.g.* biotite) during hypogene and supergene kaolinization. Ilmenite alters to microcrystalline anatase

* E-mail address of corresponding author:
papoulis@upatras.gr
DOI: 10.1346/CCMN.2009.0570505

via pseudorutile (Anand and Gilkes, 1984), but other mafic minerals, such as biotite, may also act as a source for Ti in anatase (Dill *et al.* 2006). Jiménez-Millán *et al*. (2008), studying the hydrothermally altered dolerites from the Betic Cordillera, Spain, found that biotite contained substantial amounts of Ti which may have been the source of Ti for the authigenic oxides.

Volcanic rocks cover about half of the area of Limnos Island (Davis, 1959; Fytikas *et al.*, 1980; Innocenti *et al.*, 1994) and overlie Middle Eocene to Early Miocene Flysch (Pe-Piper and Piper, 2002) (Figure 1). They include andesite, trachyandesite, trachyte, and dacite, with porphyritic plagioclase and alkali feldspar set in a microlitic groundmass of plagioclase, alkali feldspar, biotite, and quartz in variable proportions (Roussos *et al.*, 1993). Secondary phases include micas, calcite, quartz, and clay minerals. Radiometric dating of these rocks yielded ages ranging from 21 to 18.2 Ma (Fytikas *et al.*, 1984; Innocenti *et al.*, 1994). Investigations concerning the alteration of the Limnos volcanic rocks are limited, whereas more attention has been paid to their magmatic and geotectonic evolution (*e.g.* Davis, 1959; Fytikas *et al.*, 1980; Fytikas *et al.*, 1984; Innocenti *et al.*, 1994; Voudouris and Skarpelis, 1998; Koukouvelas and Aydin, 2002; Pe-Piper and Piper, 2002; Koukouvelas *et al.*, 2005; Pe-Piper *et al.*, 2009). Papoulis and Tsolis-Katagas (2008), studying the alteration of the volcanic rocks of the western and southern parts of Limnos, distinguished the formation of four types of hydrothermal alteration zones named according to the prevailing clay mineral formed as smectite-rich, illite-rich, kaolinite-dickite-rich, and halloysite-rich zones, respectively. In the same study, the formation of naturally produced nanostructured films of anatase during the hydrothermal alteration of biotite in the halloysite-rich zones of Limnos Island was discovered.

The goal of the present study was to determine the hydrothermal alteration processes which acted on the biotite in these volcanic rocks, to describe in detail the mechanism of the halloysite development, and to specify, using several diagnostic techniques, the mechanisms of formation of anatase during the alteration processes.

MATERIALS AND METHODS

Fifteen samples were collected from a halloysite-rich zone developed within the volcanic rocks in the southwestern part of Limnos Island. The sampling strategy was to collect a representative variety of samples: from the unaltered rocks, 20−30 m away from the fault; and from the most altered rocks within the fault gouge (Figure 2a). The samples were collected, stored, and examined carefully, while preserving the field-moist state in order to avoid halloysite dehydration to the 7 Å form.

The mineralogical composition of the bulk samples and of the clay fraction (<2 μm), extracted by sedimentation, were determined by X-ray powder diffraction (XRPD), using a Bruker D8 advance diffractometer, with Ni-filtered CuKα radiation. Separation of the clay fraction was carried out using centrifugation methods. Powders from oriented samples were prepared by the dropper method and were scanned at 1º2θ/min from 3 to 60º2θ. Randomly oriented powder mounts were prepared

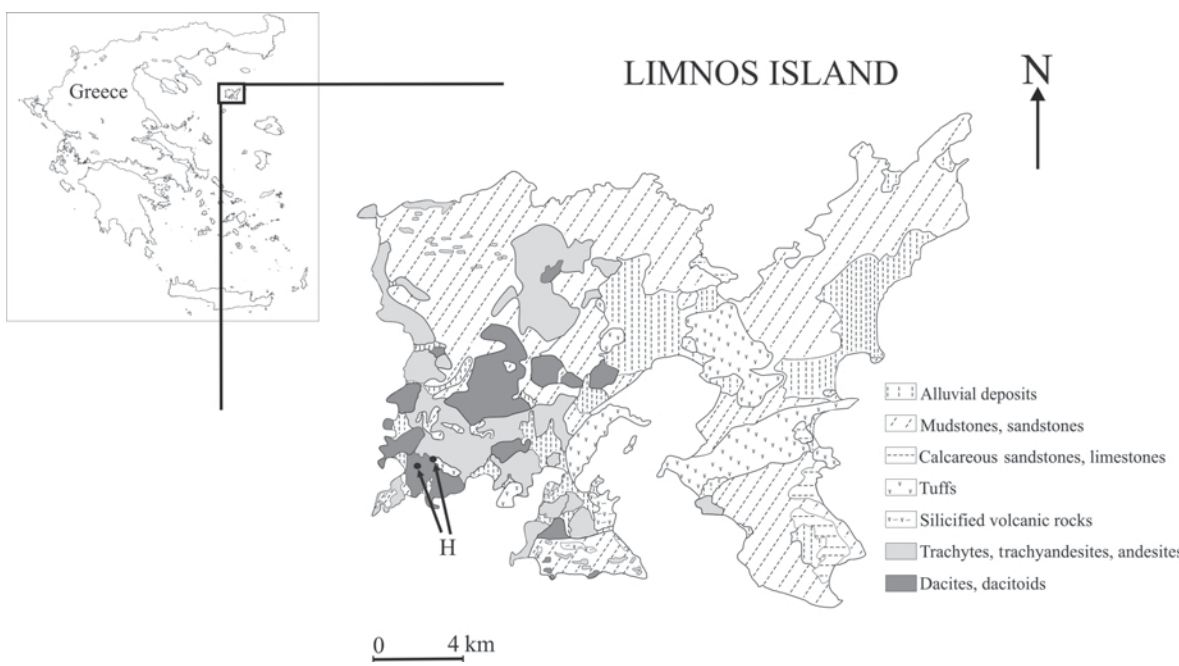

Figure 1. Geologic sketch map of Limnos island (after Roussos *et al*., 1993). H: halloysite-rich zones (indicated by arrows).

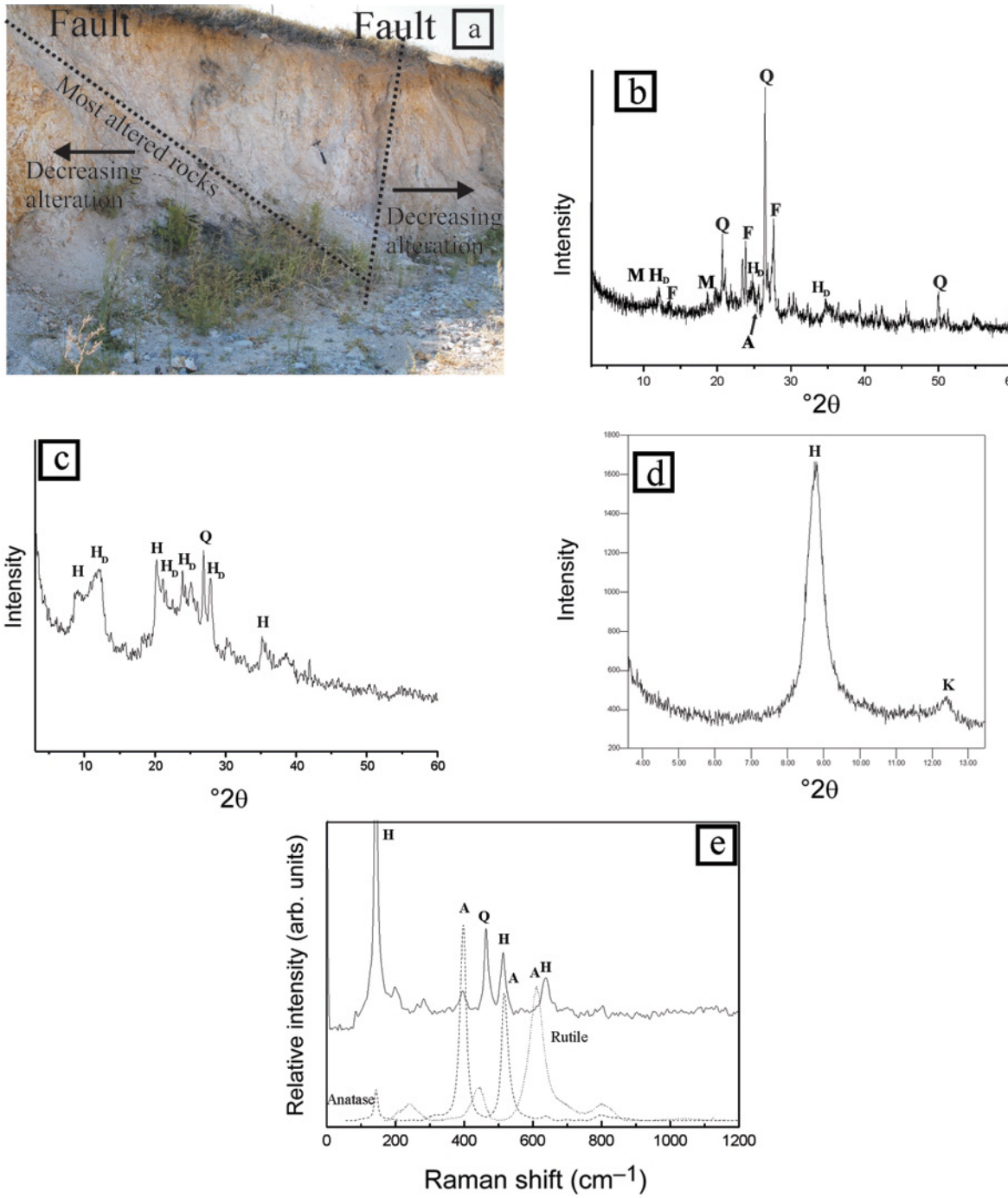

Figure 2. (a) Outcrop photo of a halloysite-rich zone; (b) XRPD pattern of a representative, moderately altered sample of this zone; (c) XRPD pattern of a representative, highly altered sample; (d) XRPD pattern of a highly altered sample after formamide treatment; (e) FT-Raman spectrum of a moderately altered sample showing the presence of halloysite (H) and anatase (A) compared with the spectra of standard anatase and rutile. H: hydrated halloysite, H_D: dehydrated halloysite, K: kaolinite, Q: quartz, F: feldspars, A: anatase, M: traces of mica.

by gently pressing the powder into the cavity holder. In order to discriminate halloysite from kaolinite, the formamide intercalation method was used (Churchman *et al.*, 1984).

Fourier-transform-Raman (FT-Raman) measurements were obtained using a Bruker (D) FRA-106/S component attached to an EQUINOX 55 spectrometer. An R510 diode pumped Nd:YAG laser at 1064 nm (with a

maximum output power of 500 mW) was used for Raman excitation in a 180º back-scattering geometry. Optical filtering reduced the Rayleigh elastic scattering and, in combination with a CaF_2 beamsplitter and a high-sensitivity liquid N_2-cooled CCD detector, allowed the Raman intensities to be recorded from 50 to 3300 cm^{-1} in a Stokes-shifted Raman region, all in one spectrum.

The clay-mineral morphology and chemical composition of coexisting minerals were examined using a JEOL 6300 Scanning Electron Microscope (SEM) equipped with an ISIS Energy Dispersive Spectrometer (EDS). The chemical composition of the minerals was determined using natural and synthetic standards. The operating conditions were 20 kV accelerating voltage and 10 nA probe current. Microanalyses were performed on epoxy resin-impregnated, carbon-coated, polished thin sections and on gold-coated or in some cases carbon-coated sample powders mounted directly on the sample holder. The clay mineral morphology was also examined using a SEM LEO SUPRA 35VP.

RESULTS

Extent, morphology, and mineralogy of the alteration

The halloysite-bearing occurrences investigated extend over an area of ~1 km^2 in the SW Limnos Island (Figure 1). Halloysite-rich zones usually occur in trachyandesites, dacites, and in some cases tuffs along both sides of a major fault and extend over a width of 20−30 m (Papoulis and Tsolis-Katagas, 2008). They are frequently cut by numerous smaller-scale faults and fractures. The alteration process is more intense close to the major fault (a few meters wide on both sides) or close to smaller faults or fractures associated with the major one (Figure 2a).

The mineralogical composition of the parent rock is characterized by the dominant presence of quartz, plagioclase, and biotite. The less altered samples contain dehydrated halloysite coexisting with quartz, feldspars, and minor amounts of micas (Figure 2b). Observations by SEM also revealed the presence of traces of zircon and monazite usually as inclusions in biotite. SEM-EDS microanalyses revealed that biotite is characterized by relatively large TiO_2 contents (up to 3 wt.%). The most altered rocks are dominated by hydrated and dehydrated halloysite and quartz (Figure 2c) while accessory zircon, monazite, crandallite-goyazite-gorceixite, and pyrite also occur (Figure 4f,g). The FT-Raman spectra (Figure 2e) revealed that halloysite is the dominant mineral phase, as illustrated by its characteristic bands at ~141 cm^{-1} and 459 cm^{-1}. Kaolinite bands at 120 cm^{-1}, 395 cm^{-1}, 426cm^{-1}, and 509 cm^{-1} (Frost, 1995, 1997) were weak. The formamide test (Churchman *et al.*, 1984) was employed to investigate the possible occurrence of kaolinite, because intense XRPD peaks, due to the predominance of halloysite, might have obscured peaks related to kaolinite (Figure 2c,d). The test revealed that, besides the occurrence of halloysite, the peak at ~7 Å also indicated the coexistence of traces of kaolinite (Figure 2d). Iron oxides, anatase, and sparse ilmenite (identified by SEM-EDS microanalyses) were present throughout the assemblage from the least to the entirely altered samples. The existence of anatase was determined using SEM-EDS, FT-Raman, and XRPD. The FT-Raman spectra suggested that the existence of other TiO_2 polytypes, including amorphous TiO_2, is not likely (Figure 2e).

Progressive stages of halloysite formation following hydrothermal alteration of biotite

Observations by SEM indicated that the alteration of biotite in the variously altered samples could be assigned to one (or in some cases two) of six distinct alteration stages. In several cases, due to their small crystal size, the precursor mica of the halloysite was not identifiable. Samples of the first stage contain dehydrated, poorly formed halloysite nanoparticles, which grew at the edges of the biotite layers. They grew on a few layers of the micas partially covering their rims and formed a thin layer ~30 nm or less thick (Figure 3a). The samples representing the second stage of alteration contained tubular halloysite, ~50 nm long (nanotubes), formed at the edges of the mica layers (Figure 3b). Compared to the samples of the first stage, the halloysite tubes are longer (0.5−1 μm), cover a greater area at the edges of the layers, and, infrequently, extend slightly into the inner parts of the layers (Figure 3c). The third stage of alteration is recognized in samples containing tubes and laths of halloysite up to 2 μm long (Figure 3d), which are usually parallel to the layers of their precursor biotite. The alteration expands slightly over the inner parts of the biotite flakes and some holes are visible in the biotite layers. Because of the small size of the halloysite crystals, reliable quantitative microanalyses were impossible so only qualitative SEM-EDS microanalyses back up the SEM observations. A significant number of such analyses on dense aggregates of tubular halloysite showed a rather unusual chemical composition, characterized by significant Ti content (Figure 5g). An uncertainty arises, however, as to whether this Ti content is actually a chemical constituent of the halloysite or if it reflects Ti-contaminated analyses affected by an unobservable or intermingled Ti-bearing phase. Nevertheless, in most of the analyses, the formula of halloysite showed no tetrahedral or octahedral substitutions. The samples of the fourth alteration stage include only relics of micas, because most were significantly altered to halloysite, forming tubes, laths, and interconnected tubes (Figure 3e). Numerous holes are visible in the inner parts of the mica layers. The fifth stage is characterized by the presence of traces of micas while most of the mica layers have been altered to halloysite tubes and laths. Interconnected laths and tubes dominate the crystal habit of halloysite (Figure 3f).

These newly formed tubes and laths of halloysite form dense aggregates, developing in thin layers which mimic the layered morphology of the micas (Figure 3f,g). In the samples representing the final, sixth stage of alteration, micas are completely altered to halloysite having a prevailing morphology of interconnected laths and tubes (Figure 3h). Very commonly the parallel connection of partially unified halloysite laths leads to the formation of platy forms (Figure 3f).

Typically, most of the halloysite tubes from all stages of alteration show a hollow interior, ~30 nm in diameter, which are mostly empty but in some cases they are occupied by stacked, poorly formed halloysite tubes. In some cases, they are longer than their host crystals extending in one and rarely even in both directions (Figure 3b,c,e,f,g,h). The average calculated structural formula, after SEM-EDS micranalyses, of the laths and interconnected laths of halloysite is $(Al_{3.96}Fe_{0.04})Si_4O_{10}(OH)_8$.

Formation of anatase

Anatase is encountered as an alteration product of both ilmenite and biotite. Ilmenite crystals (identified by SEM-EDS) were partially altered to anatase and Fe oxides (Figure 4a); the latter are usually distributed in areas surrounding the ilmenite crystals. As alteration progressed, ilmenite was diminished while parallel layers of anatase became more abundant and easily recognized (Figure 4b,c). In the intensively altered rocks of stages four to six, spaces between anatase layers were filled with tubes and laths of halloysite (Figure 4d,e). Rarely, partially altered monazite and/or its alteration product crandallite-goyazite-gorceixite were also detected by SEM-EDS within these spaces (Figure 4f,g).

Anatase was also formed from the alteration of biotite. Even in the least altered samples, platy anatase nanoparticles occurred between mica layers (Figure 5a). The nanoparticles were enhanced with increasing alteration and were connected to create platy forms aligned parallel to the mica layers (Figure 5b). In the extremely altered rocks, the anatase layers were covered by halloysite (Figure 4e). As for halloysite, the formation of anatase was mostly confined to the edges of the biotite layers and progressively occupied the inner parts of the mica layers, surrounding holes left in mica layers due to the formation and detachment of halloysite tubes (Figure 5c). From that stage forward, anatase nanoparticles were then connected to each other on the periphery of the cavities in micas, forming unusual ring shapes (Figure 5d). These rings were stacked and set in planes approximately parallel to former biotite layers, which were subsequently altered to halloysite (Figure 5e,f).

DISCUSSION

The alteration processes in the intermediate to acid volcanic rocks at Limnos Island are spatially associated with a major fault zone. Halloysite is abundant in all the collected samples along this alteration zone. The mode of occurrence of the halloysite-rich zones, coupled with the morphology of the halloysite, strongly suggests a low-temperature, hydrothermal origin. Halloysite crystals can adopt a variety of morphologies (Kunze and Bradley, 1964; de Souza Santos *et al.*, 1966; Dixon and McKee, 1974; Tazaki, 1982; Wada and Mizota, 1982; Churchman and Theng, 1984; Noro, 1986; Bailey, 1990; Papoulis *et al.*, 2004b), the most common of which is the elongate tubule (Joussein *et al.*, 2005). The morphological variability of halloysite is attributed to various factors, including crystal structure, degree of alteration, chemical composition, and the effects of dehydration (Joussein *et al.*, 2005). The dominant morphology of the Limnos halloysite is tubular in the less and moderately altered samples (stages 1–3); interconnected tubular halloysite was detected in samples of the fourth to sixth alteration stages. The observed similarities, especially in terms of morphology (*e.g.* presence of both open-hole with similar size of hollow interior and closed-hole tubular halloysite), between halloysite from Limnos Island and hydrothermal halloysite from the Turplu area, Turkey (Ece and Schroeder, 2007; Ece *et al.*, 2008), and the gradual increase in the degree of alteration closer to the fault, suggest the involvement of hydrothermal fluids in the formation of halloysite in the studied area.

The formation of the low-temperature TiO_2 polymorph, anatase, rather than rutile, along with its small-particle diameter (Zhang and Banfield, 1998), also favor a hydrothermal, low-temperature origin for the alteration zones. According to Utada (1980) and Ece *et al*. (2008), the hydrothermal formation of kaolinite after halloysite is favored at temperatures at or <100ºC, while Ece *et al*. (2008) showed that halloysite can form at temperatures

Figure 3 (*facing page*). SEM images showing: (a) poorly formed, dehydrated halloysite nanoparticles grown at the edges of biotite (arrows); (b) tubular halloysite, ~50 nm long, forming at the edges of biotite layers (arrows); (c) biotite layers characterized by the alteration of their edges to tubular halloysite (arrow). The tubes are ~0.5–1 μm long; spheroidal forms are of anatase; (d) biotite layers altered to relatively large (up to 2 μm) halloysite tubes and laths (arrow); (e) layers of micas largely altered to laths, tubular and interconnected tubular halloysite; inset: EDS analysis of the latter. Most of the halloysite tubes have a hollow interior but some of the tubes are filled; the spheroidal form is of anatase; (f,g) micas largely altered to laths and to tubular and interconnected tubular halloysite; inset: EDS analyses of halloysite. The arrows indicate mica remnants. (h) Partially unified laths and interconnected laths of halloysite forming platy forms and EDS analysis on halloysite. h: halloysite tubes with a hollow interior; o: filled halloysite tubes; B: biotite.

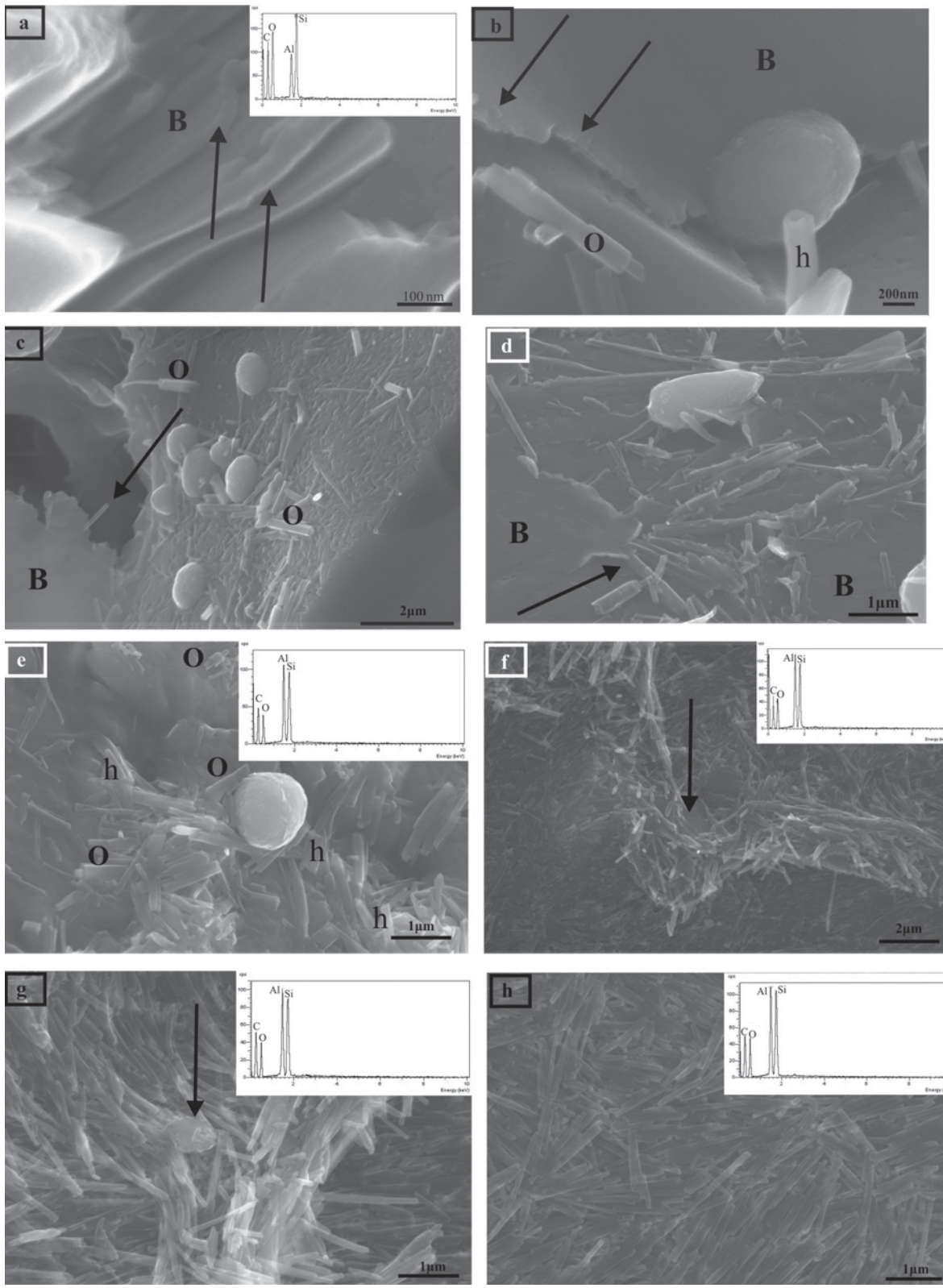
a
O
C
Si
Al
B
100 nm
b
B
O
h
200nm
c
O
O
B
2μm
d
B
B
1μm
e
O
Al
Si
C
O
h
O
O
h
h
1μm
f
Al
Si
C
O
2μm
g
Al
Si
C
O
1μm
h
Al
Si
C
O
1μm

as high as 150ºC only when it coexists with alunite, hence the absence of alunite indicates the temperature of formation of the halloysite at Limnos was at or <100ºC. Moreover, halloysite is commonly considered to be unstable in weathering environments where it reacts to form kaolinite (*e.g.* Dong *et al.*, 1998; Papoulis *et al.*, 2004a). Due to the fact that kaolinite occurs only in traces in the studied samples, it is unlikely that weathering could account for the alteration mechanism in the volcanic rocks. The tightly packed tubes and laths of halloysite indicate limited space available, which is, again, in line with a hydrothermal origin. Apart from the hydrothermal fluids, the crystal structure, morphology, and cleavage of the altered micas and the degree of the alteration must have played an important role in the genesis of these halloysite forms.

Most of the titanium needed for the formation of anatase was released from the alteration of ilmenite and only a small amount could be attributed to the alteration of micas, especially of biotite (SEM-EDS analyses of biotite grains showed Ti content of up to 3 wt.%). Minor amounts of Ti could also have been provided by the alteration of other minerals (*e.g.* plagioclase) or from the implicated hydrothermal fluid phase. The altered ilmenite crystals constrain most of the newly formed anatase within the space previously occupied by the unaltered ilmenite, thus leading to the formation of skeletal anatase (Figure 6, I, II, III). The layered structure of biotite, however, seems to be the main determining factor for the morphology of newly formed anatase that is not constrained within the altered ilmenite, resulting in patterns of anatase layers parallel to mica layers (Figure 6 alteration stages 1–6). The formation of anatase rings derives from the alteration of biotite to tubular halloysite within the inner parts of the biotite layers, during the alteration stages 4 to 6. The observed, newly formed, tubular halloysite crystals growing with their long axes perpendicular to the biotite layers are rather unusual. These crystals can be detached easily from the biotite layers by hydrothermal fluids, leaving behind holes in the inner parts of the flakes. Ring-shaped anatase formed subsequently around the holes. The above procedure could only take place within open folia where the halloysite tubes were given space to grow perpendicular to mica layers and hydrothermal fluids could enter easily. As the alteration of biotite proceeded further and the number of detached halloysite crystals increased, several stacking groups of parallel anatase rings appeared. Again, the planar structure of biotite governed the pattern of the anatase rings because the latter formed parallel to and between the biotite layers. Hydrothermal fluid circulation occurred more easily between open folia, thus explaining the remains of the rings in the most altered samples and the absence of anatase cylinders.

A significant number of halloysite microanalyses showing consistent but unusually large Ti contents cannot be realistic because it is well known that halloysite cannot incorporate Ti in its structure (Joussein *et al.*, 2005) and an uncertainty arises as to whether this Ti content is actually a chemical constituent of the halloysite, or if it reflects Ti-contaminated analyses affected by an unseen or intermingled Ti-bearing phase. A plausible explanation for these unusual compositions is that the halloysite analyses are biased by microscopic anatase crystals. This explanation is further supported by the fact that X-ray spectra obtained from halloysite tubes or laths covering visible anatase layers clearly show Ti peaks (Figure 5g). Depending on the inclination of an anatase layer relative to the surface of the polished-thin section, the acquired microanalysis of a halloysite may implicate variable degrees of undesirable contributions from anatase grains at depth within the interaction volume of the X-ray beam. The constant composition of Ti in the halloysite analyses obtained may be explained by assuming that anatase layers lie parallel to and between the halloysite layers, thus equally biasing the results.

CONCLUSIONS

Hydrothermal alteration of trachyandesites, dacites, and tuffs in SW Limnos Island resulted from the hydrothermal circulation of fluids through multiple faults and fractures, located along a major fault zone. The formation of halloysite after biotite suggested low-temperature alteration (~80ºC) while the subsequent formation of minor kaolinite indicated the involvement of hydrothermal fluids at ~100ºC. Hydrothermal fluids at this temperature caused concomitant hydrothermal alteration of ilmenite to anatase. The alteration of biotite to halloysite tubes, laths, and interconnected laths follows six discrete stages. Nanoparticles of halloysite formed at the expense of biotite layers and grew progressively through short-tubular halloysite towards well formed tubular halloysite. In the most altered samples, tubular halloysite converted to laths and interconnected laths of halloysite while biotite was completely altered. The altered ilmenite crystals constrained the growth of the newly formed anatase leading

Figure 4 (*facing page*). (a–f) BSE-SEM images showing: (a) an altered ilmenite crystal (I) filled with a newly formed anatase layer and Fe oxides; (b,c) altered ilmenite crystals; ilmenite is depleted in Fe and the development of parallel anatase layers (arrows) is easily recognized; (d,e) close-up view of an altered ilmenite crystal; Fe is depleted and the space between anatase layers (arrows) is filled with halloysite tubes and laths (H); (f) crandallite-goyazite-gorceixite; (g) SEM image showing crandallite-goyazite-gorceixite (CGG) along with halloysite.

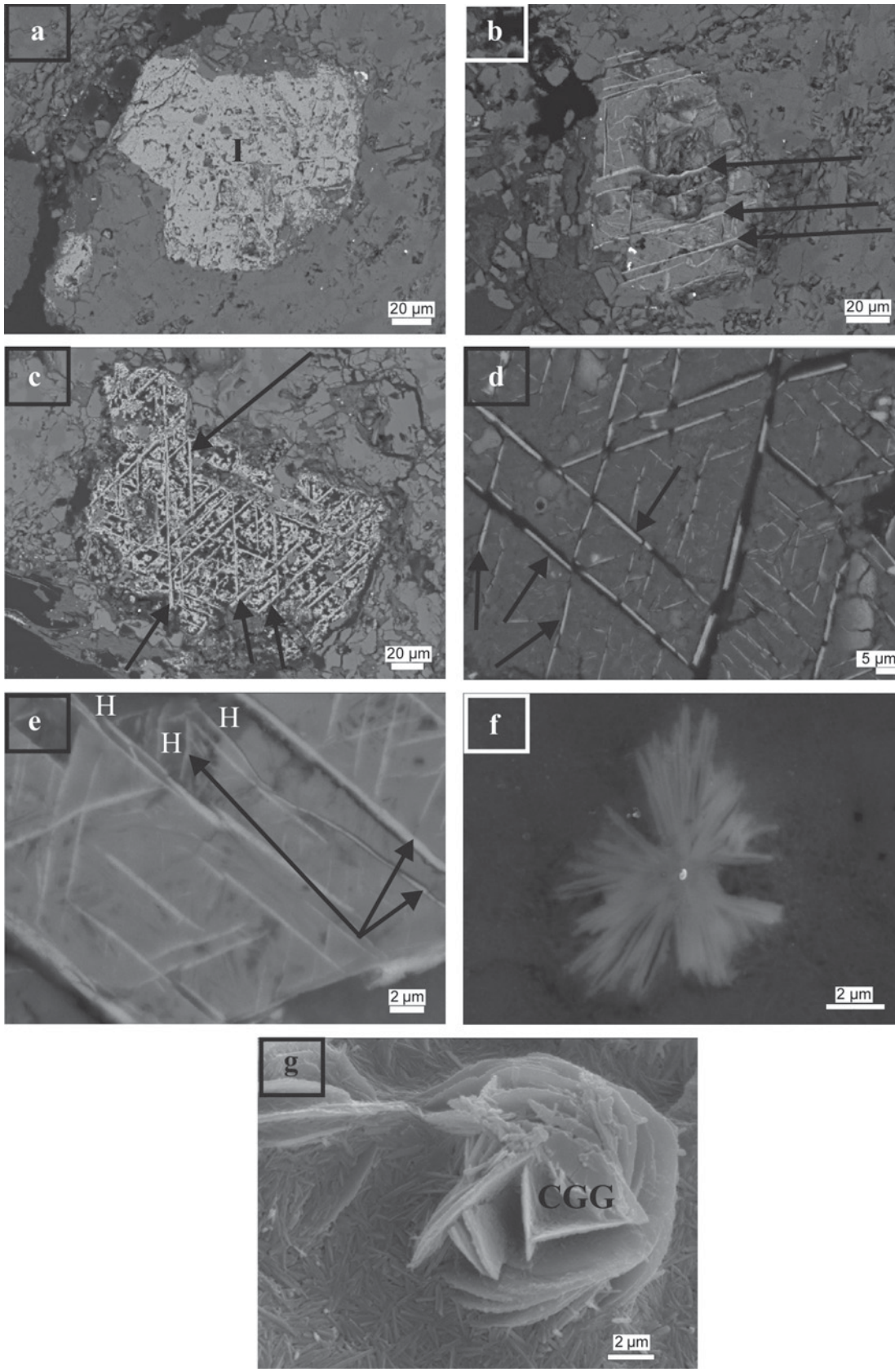
a
I
20 μm
b
20 μm
c
20 μm
d
5 μm
e
H
H
H
2 μm
f
2 μm
g
CGG
2 μm

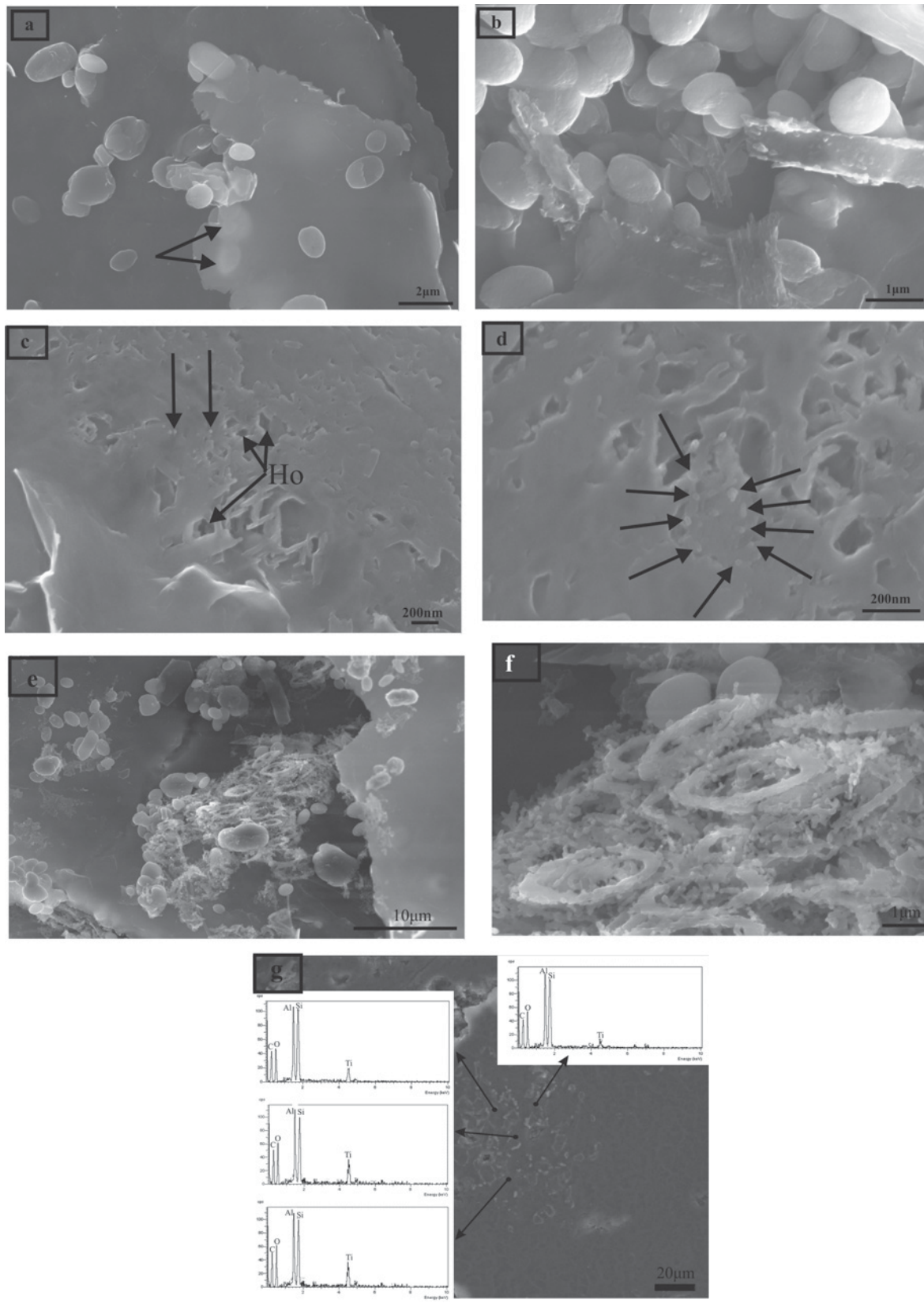
a
2μm
b
1μm
c
Ho
200nm
d
200nm
e
10μm
f
1μm
g
Al
Si
O
C
Ti
20μm

Figure 5 (*facing page*). SEM images showing: (a) platy anatase forms (arrows) consisting of nanoparticles formed between mica layers; (b) connected platy forms of anatase arranged parallel to the mica layers; (c) holes (Ho) in mica layers due to the formation and detachment of halloysite tubes (arrows); (d) connected anatase nanoparticles in ring-like form around the rims of holes in mica layers while new halloysite tubes are formed (arrows); (e,f) ring-like forms of anatase nucleating mostly parallel to each other and to the remnant unaltered and pre-existing biotite layer substrate; (g) halloysite tubes and laths cover anatase layers; inset: EDS analyses

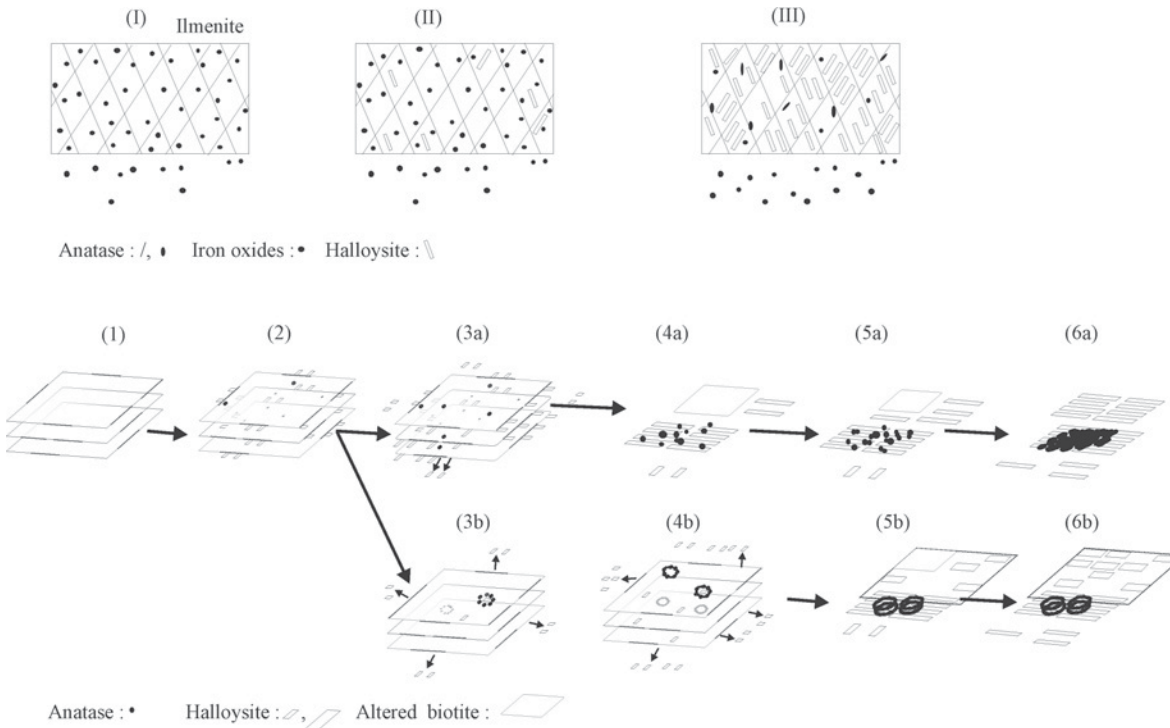

Figure 6. Schematic representation of the first, second, and third stages of the alteration of ilmenite. (a,b) Schematic representation of the six stages of the alteration of mica layers and the formation mechanisms of halloysite and anatase (see text for details).

to the initial formation of skeletal anatase. The layered structure of micas was the main factor controlling the morphology of the newly formed anatase not otherwise constrained by the ilmenite crystals. As a result, parallel anatase layers were formed between mica layers. In the final stages of alteration, anatase formed unusual ring patterns around holes in mica flakes after the detachment of halloysite crystals growing perpendicular to the mica planes caused by hydrothermal fluids. The above procedure can only take place within exfoliated micas where the halloysite tubes would have the space to grow at right angles to the mica layers and the hydrothermal fluids could circulate easily.

ACKNOWLEDGMENTS

The authors thank Dr Drakopoulos of the Foundation for Research and Technology-Hellas (FORTH), Institute of Chemical Engineering and High Temperature Chemical Processes (ICE/HT), Rio-Patras, Greece, and Mr Kotsopoulos, of the Laboratory of Electron Microscopy and Microanalysis, University of Patras, for their help with the scanning electron microscopy.

REFERENCES

Ahn, J.H. and Peacor D.R. (1987) Kaolinitization of biotite: TEM data and implications for an alteration mechanism. *American Minereralogist*, **72**, 353–356.

Anand, R.R. and Gilkes, R.J. (1984) Weathering of hornblende, plagioclase and chlorite in meta-dolerite, Australia. *Geoderma*, **34**, 261–280.

Arostegui, J., Irabien, M.J., Nieto, F., Sangüesa, J., and Zuluaga, M.C. (2001) Microtextures and the origin of muscovite-kaolinite intergrowths in sandstones of the Utrillas Formation, Basque Cantabrian Basin, Spain. *Clays and Clay Minerals*, **49**, 529–539.

Bailey, S.W. (1990) Halloysite – A critical assessment. Pp. 89–98 in: *Crystal Structure and Mixed Layering of Clays*. Proceedings of the 9th International Clay Conference 1989 (V.C. Farmer and Y. Tardy, editors). Mémoire 86, Science Géologiques, Strasbourg, France.

Banfield, J.F. and Eggleton, R.A. (1990) Analytical transmission electron microscope studies of plagioclase, muscovite, and K-feldspar weathering. *Clays and Clay Minerals*, **38**, 77–89.

Chen, P.Y., Lin, M.L., and Zheng, Z. (1997) On the origin of the name kaolin and the kaolin deposits of the Kauling and Dazhou areas, Kiangsi, China. *Applied Clay Science*, **12**, 1–25.

Churchman, G.J. and Theng, B.K.G. (1984) Interactions of

halloysites with amides: Mineralogical factors affecting complex formation. *Clay Minerals*, **19**, 161–175.

Churchman, C.J., Whitton, J.S., Claridge, G.G.C., and Theng, B.K.G. (1984) Intercalation method using formamide for differentiating halloysite from kaolinite. *Clays and Clay Minerals*, **32**, 241–248.

Davis, E. (1959) Volcanic rocks of Limnos, island. *Annales Geologiques des Pays Helleniques*, **11**, 1–83 (in Greek).

de Souza Santos, P., de Souza Santos, H., and Brindley, G.W. (1966) Mineralogical studies of kaolinite-halloysite clays: part IV. A platy mineral with structural swelling and shrinking characteristics. *American Mineralogist*, **51**, 1640–1648.

Dill, H.G., Bosse, H.-R., Henning, K.-H., Fricke, A., and Ahrend, H. (1997) Mineralogical and chemical variations in hypogene and supergene kaolin deposits in a mobile fold belt – The Central Andes of northwestern Peru. *Mineralium Deposita*. **32**, 149–163.

Dill, H.G. Melcher, F. Füßl, M., and Weber B. (2006) Accessory minerals in cassiterite: A tool for provenance and environmental analyses of colluvial–fluvial placer deposits (NE Bavaria, Germany). *Sedimentary Geology*, **191**, 171–189

Dixon, J.B. (1989) Kaolin and serpentine group minerals. Pp. 467–526 in: *Minerals in Soil Environments*, 2nd edition (J.B. Dixon and S.B. Weed, editors). Soil Science Society of America, Madison, Wisconsin, USA.

Dixon, J.B. and McKee, T.R. (1974) Internal and external morphology of tubular and spheroidal halloysite particles. *Clays and Clay Minerals*, **22**, 127–137.

Dong, H., Peacor, D.R., and Murphy, S.F. (1998) TEM study of progressive alteration of igneous biotite to kaolinite throughout a weathered soil profile. *Geochimica et Cosmochimica Acta*, **62**, 1881–1887.

Ece, Ö.I. and Schroeder, P.A. (2007) Clay mineralogy and chemistry of halloysite and alunite deposits in the Turplu area, Balikesir, Turkey. *Clays and Clay Minerals*, **55**, 18–35.

Ece, Ö.I., Schroeder, P.A., Smilley, M.J., and Wampler, J.M. (2008) Acid-sulphate hydrothermal alteration of andesitic tuffs and genesis of halloysite and alunite deposits in the Biga Peninsula, Turkey. *Clay Minerals*, **43**, 281–315.

Frost, R.L. (1995) Fourier Transform Raman spectroscopy of kaolinite, dickite and halloysite. *Clays and Clay Minerals*, **43**, 191–195.

Frost, R.L. (1997) The structure of the kaolinite minerals – a FT-Raman study. *Clay Minerals*, **32**, 65–77.

Fytikas, M., Giuliani, O., Innocenti, F., Manetti, P., Mazzuoli, R., Peccerillo, A., and Villari, L. (1980) Neogene volcanism of the northern and central Aegean region. *Annales Geologiques des Pays Helleniques*, **30**, 106–129.

Fytikas, M., Innocenti, F., Manetti, P., Mazzuoli, R., Peccerillo, A., and Villari, L. (1984) Tertiary to Quaternary evolution of volcanism in the Aegean region. Pp. 687–699 in: *The Geological Evolution of the Eastern Mediterranian* (J.E. Dixon and A.H.F. Robertson, editors). Special Publications, **17,** Geological Society, London.

Giese, R.F. (1988) Kaolin minerals: Structures and stabilities. Pp. 29–66 in: *Hydrous Phyllosilicates (Exclusive of Micas)* (S.W. Bailey, editor). Reviews in Mineralogy, **19**, Mineralogical Society of America, Washington, D.C.

Harvey, C.C. and Murray, H.H. (1993) The geology, mineralogy, and exploitation of halloysite clays of Northland, New Zealand. Pp. 233–248 in: *Kaolin Genesis and Utilization* (H.H. Murray, W.M. Bundy, and C.C. Harvey, editors*)*. Special Publications, **1**, The Clay Minerals Society, Bloominton, Indiana, USA.

Innocenti, F., Manetti, P., Mazzuoli, R., Pertusati, P., Fytikas, M., and Kolios, N. (1994) The geology and geodynamic significance of the island of Limnos, North Aegean sea, Greece. *Neues Jahrbuch für üGeologie Paläont. Monatshefte*, **11**, 661–691.

Jiang, W. and Peacor, D.R. (1991) Transmission electron microscopic study of the kaolinitization of muscovite. *Clays and Clay Minerals*, **39**, 1–13.

Jiménez-Millán, J., Abad, I., and Nieto, F. (2008) Contrasting alteration processes in hydrothermally altered dolerites from the Betic Cordillera, Spain. *Clay Minerals*, **43**, 267–280.

Jolicoeur, S., Ildefonse, P., and Bouchard, M. (2000) Kaolinite and gibbsite weathering of biotite within saprolites and soils of Central Virginia. *Soil Science Society of America Journal*, **64**, 1118–1129.

Joussein, E., Petit, S., Churchman, J., Theng, B., Righi, D., and Delvaux, B. (2005) Halloysite clay minerals – a review. *Clay Minerals*, **40**, 383–426.

Kirkman, J.H. (1981) Morphology and structure of halloysite in New Zeland tephras. *Clays and Clay Minerals*. **29**, 1–9.

Koukouvelas, I. and Aydin, A. (2002) Fault structure and related basins of the North Aegean Sea and its surroundings. *Tectonics*, **21**, 10.1029/2001TC 901037.

Koukouvelas, I.K., Pe-Piper G., Piper, D.J.W., Kokkalas, S., and Dolansky, L. (2005) Miocene volcanism of Limnos, NE Greece. Pp. 53–54 in: *Geology of Thrace and Seismotectonics of NE Aegean Sea*. Samothrace, Greece.

Kunze, G.W. and Bradley, W.F. (1964) Occurrence of a tabular halloysite in a Texas soil. Pp. 523–528 in: Proceedings of the 12th National Conference on Clays and Clay Minerals 1963 (W.F. Bradley, editor). *Clays and Clay Minerals*, **19**, Pergamon Press, Oxford, UK.

Murray, H.H. and Keller, W.D. (1993) Kaolin, kaolin and kaolin. Pp. 1–24 in: *Kaolin Genesis and Utilization* (H.H. Murray, W. Bondy, and C. Harvey, editors). Special Publications, **1**. The Clay Minerals Society.

Noro, H. (1986) Hexagonal platy halloysite in an altered tuff bed, Komaki city, Aichi prefecture, Central Japan. *Clay Minerals*, **21**, 401–415.

Papoulis, D. and Kalampounias, A.G. (2008) Naturally produced anatase nanostructured films during the hydrothermal alteration of biotite. Proceedings of the IASTED International Conference *Nanotechnology and Applications* (NANA 2008), pp. 157–162.

Papoulis, D. and Tsolis-Katagas, P. (2008) Formation of alteration zones and kaolin genesis, Limnos island, Northeast Aegean Sea, Greece. *Clay Minerals*, **43**, 631–646.

Papoulis, D., Tsolis-Katagas, P., and Katagas, C. (2004a) Monazite alteration mechanisms and depletion measurements in kaolins. *Applied Clay Science*, **24**, 271–285.

Papoulis, D., Tsolis-Katagas, P., and Katagas, C. (2004b) Progressive stages in the formation of kaolin minerals of different morphologies in the weathering of plagioclase. *Clays and Clay Minerals*, **52**, 275–286.

Pe-Piper, G. and Piper, D.J.W. (2002) *The Igneous Rocks of Greece. The Anatomy of an Orogen.* Gebrüder Borntraeger, Berlin, Stuttgart.

Pe-Piper, G., Piper, D.J.W., Koukouvelas, I., Dolansky, L.D., and Kokkalas, S. (2009) Postorogenic shoshonitic rocks and their origin by melting underplated basalts: The Miocene of Limnos, Greece. *GSA Bulletin*, **121**, 39–54.

Quantin, P., Gautheyron, J., and Lorenzoni, P. (1988) Halloysite formation through in situ weathering of volcanic glass from trachytic pumices, Vico's volcano, Italy. *Clay Minerals*, **23**, 423–437.

Roussos, N., Katsaounis, A., Tsaila-Monopoli, S., Ioakeim, X, Karadasi, S., and Davi, E. (1993) *Geological Map of Limnos Island*. Institute of Geology and Mineral Exploration, Greece.

Schroeder, P.A. and Shiflet, J. (2000) Ti-bearing phases in the Huber Formation: an east Georgia kaolin deposit. *Clays and*

Clay Minerals, **48**, 151–158.
Singh, B. and Gilkes, R.J. (1992) An electron optical investigation of the alteration of kaolinite to halloysite. *Clays and Clay Minerals*, **40**, 212–229.
Tazaki, K. (1982) Analytical electron microscopic studies of halloysite formation processes: morphology and composition of halloysite. Pp. 573–584 in: *Proceedings of the 7th International Clay Conference 1981* (H. Van Olphen and F. Veniale, editors). Developments in Sedimentology, **35**, Elsevier, Amsterdam.
Utada, M. (1980) Hydrothermal alteration related to igneous acidity in Cretaceous and Neogene formations of Japan. *Mining Geology of Japan, Special Issue*, **12**, 79–92.
Voudouris, P. and Skarpelis, N. (1998) Epithermal gold-silver mineralizations at Perama (Thrace) and Lemnos island [in Greek, English abstract]. *Bulletin of the Geological Society of Greece*, **32**, 125–135.
Wada, S.I. and Mizota, C. (1982) Iron-rich halloysite (10 Å) with crumpled lamellar morphology from Hokkaido, Japan. *Clays and Clay Minerals*, **30**, 315–317.
Weaver, C.E. (1976) The nature of TiO_2 in kaolinite. *Clays and Clay Minerals*, **24**, 215–218.
Zhang, H. and Banfield, J.F. (1998) Thermodynamic analysis of phase stability of nanocrystalline titania. *Journal of Materials Chemistry*, **8**, 2073–2076.

(*Received 3 July 2008; revised 24 March 2009; Ms. 0180; A.E. M.A. Velbel*)